Macromolecules

ARTICLE

pubs.acs.org/Macromolecules

# Effect of $TiO_2$ Formation on the Free Volume Properties of Electrospun PMMA Nanohybrids

Junhua Zhang,[†] Mingshu Yang,[*,†] and Frans H. J. Maurer[*,‡]

[†]Beijing National Laboratory for Molecular Sciences, Key Laboratory of Engineering Plastics, Institute of Chemistry, Chinese Academy of Sciences, Beijing 100190, China

[‡]Polymer & Materials Chemistry, Department of Chemistry, Lund University, SE-22100 Lund, Sweden

**ABSTRACT:** Positron annihilation lifetime spectroscopy (PALS) has been performed on a series of PMMA nanohybrids containing nanometric $TiO_2$, which were produced by means of different preparation methods, i.e., melt mixing, electrospinning combined with solution mixing, or in-situ sol−gel growth methods, to study the effect of filler content and constituents on the free volume properties. The PMMA nanocomposites containing titania precursor or in-situ-formed $TiO_2$ additives exhibit altered free volume properties compared to adding commercial $TiO_2$ P25 fillers. The orthopositronium (o-Ps) lifetime ($\tau_3$) (free volume cavity size) was constant with composition in P25/PMMA nanohybrids due to the absence of interfacial interaction. However, in $TiO_2$ precursor/PMMA composite fibers the free volume cavity size decreased substantially with hydroxyl group concentration and recovered after hydrothermal treatment. Additionally, a strong correlation between the glass transition temperature and the o-Ps lifetime in the nanohybrids was observed. These effects are caused by the hydrogen-bonding interaction between hydroxyl groups in the inorganic phase and carbonyl groups in the PMMA matrix, which concentration is dependent on the hydrothermal treatment, leading to differences in the packing of the polymer chains and a changed polymer segmental flexibility. The results also show a clear linear decrease in the o-Ps yield ($I_3$) with increasing P25 content of the composites. A dominant inhibition effect was observed in the $TiO_2$ precursor/PMMA systems, caused by inhibition of positronium formation by the hydroxyl group in the titania precursor. In addition to the pronounced negative deviations of the o-Ps intensity with the concentration of hydroxyl groups in in-situ $TiO_2$/PMMA nanohybrid fibers, a stronger inhibition efficiency of hydroxyl groups was observed than in the precursor/PMMA nanocomposite fibers.

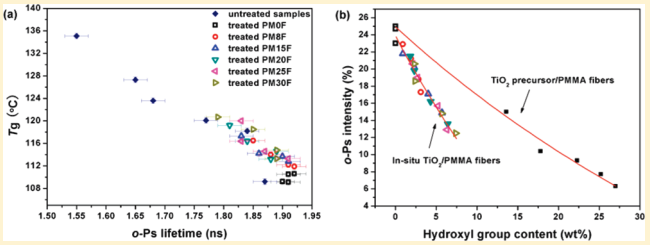


## 1. INTRODUCTION

Organic−inorganic nanohybrid materials have attracted considerable attention for their potential applications in many fields due to their extraordinary multifunctional properties, such as increased mechanical strength, improved gas permselectivity, and enhanced thermal and electrical properties.[1−11] The direct mixing of the inorganic micro- or nanosized fillers into a polymer matrix is the most simple and extensive method used. However, important aspects when introducing high-surface-area fillers into a polymer matrix are the limited dispersion of the filler particles and the closely linked interfacial interaction between filler and polymer matrix.[12−15] Weak interfacial interaction can lead to the formation or preservation of filler aggregates. Alternatively, in the past decades much effort has been devoted to developing new composite materials produced by modifying polymers via the incorporation of a variety of inorganic additives by a sol−gel method. The composites can be generated by reacting an inorganic alkoxide directly with an organic polymer or an oligomer which have the appropriate functional groups, thus providing covalent linkages between the organic segment and the inorganic network.[16−25] Especially, in-situ polymerization of an alkoxide within a swollen polymer network can be used to form organic−inorganic hybrid materials without covalent cross-links.[26−36] The size and dispersion of the inorganic phase depend on the specific sol−gel conditions, the type of alkoxide, and the nature of molecular interactions between the polymer and the inorganic oxide. Excellent dispersion can be achieved on a nano scale, particularly with polymers containing functional groups such as carbonyls, hydroxyls, or ether oxygens, which can form hydrogen bonds with the inorganic network.[30−34]

In recent years, electrospun fibers have gained a growing interest in applications such as alternative nanotemplates for fabricating nanostructures, filters, catalysis, and chemical and biological sensors. Owing to their low dimensions, large surface areas, and small pore sizes, the fibers can be used as nonwoven fabrics.[37−47] Electrospinning combined with a sol−gel method has been employed to prepare nanohybrid fibers containing inorganic nanoparticles due to its versatility and easy process control.[48−55] Recently, for the first time, $TiO_2$ nanoparticles with a mean diameter of 5 nm were in-situ generated in one-dimensional

**Received:** May 3, 2011
**Revised:** June 8, 2011
**Published:** June 22, 2011

PMMA nanohybrid fibers with excellent dispersion by using a suitable mixture of solvents with the combined technique, followed by a mild hydrothermal treatment that avoids high-temperature treatments and therefore does not affect negatively the properties of the polymer.[56]

The structure and morphologies have been investigated by means of FTIR, XPS, TGA, and DSC. The acid cosolvent trifluoracetic acid (TFA) and the fast electrospinning process induced stable titania precursor/PMMA nanocomposite fibers owing to the hydrogen-bonding interaction between the constituents. The fibrous nanoscale template facilitated the homogeneous growth of $TiO_2$ in the PMMA matrix. As a result, the phase separation of the nanohybrids was restrained by the hydrogen-bonding interaction between residual hydroxyl groups on the surface of titania and carbonyl groups in PMMA.

Using techniques such as nuclear magnetic resonance,[57−59] dielectric spectroscopy,[60,61] differential scanning calorimetry,[62−64] and positron annihilation lifetime spectroscopy,[65−70] it has been observed that the interactions between polymer segments and surfaces of inorganic fillers may induce altered chain dynamics and glass transition temperatures. The changes in chain dynamics and glass transition temperature are most probably related to the conformational changes, changes in segmental mobility, and therefore also changes in free volume structure of the polymer. The free volume sites of a polymer form the space available for segmental motions, such as the large-scale motions associated with the glass transition.

At present, positron annihilation lifetime spectroscopy (PALS) has become an increasingly important technique to detect atomic-scale free volume holes of polymers, which probes the size of the free volume cavities of the polymer by measuring the mean lifetime of orthopositronium (o-Ps) before annihilation in the free volume regions of the polymer. The lifetime of o-Ps (usually 1−5 ns) is a direct measure of the free volume cavity size. When a positron emitted from a radioactive source enters a polymer sample, it may take part in three different annihilation processes. A positron can annihilate directly with an electron in ∼0.4 ns. It can also form a metastable "atom" with a free electron, which is called positronium (Ps). Depending on the spins of the positron and electron, para- or orthopositronium is formed. In parapositronium (p-Ps), the spins of the electron−positron pair are antiparallel and p-Ps annihilates in 0.125 ns, whereas the lifetime of orthopositronium (o-Ps), in which the spins are parallel, is 142 ns in vacuum. In polymers, o-Ps is formed or diffuses to low electron dense free volume sites. The vacuum o-Ps lifetime is then reduced to 1−5 ns, due to the pick-off process of the positron with an electron of opposite spin at the free volume cavity wall. This process is called "pick-off" annihilation. The pick-off annihilation lifetime is inversely proportional to the overlap of the positron and electron wave functions and can thus be related to the size of the low-electron-density site at which the annihilation takes place.[71] A semiempirical equation, the Tao−Eldrup equation, is used to calculate the mean free volume hole radius from the measured mean o-Ps lifetime ($\tau_3$):[72,73]

$$\tau_3 = 0.5\left(1 - \frac{R}{R+\Delta R} + \frac{1}{2\pi}\sin\frac{2\pi R}{R+\Delta R}\right)^{-1} \quad (1)$$

This model assumes spherical cavities of radius $R$ with an electron layer thickness of $\Delta R$. Nakanishi et al.[74] derived a $\Delta R$ value of 0.166 nm for materials, such as polymers, containing simple covalent bonds.

The o-Ps formation probability is called o-Ps intensity $I_3$ and is primarily determined by the availability of electrons with which a positron can combine to form positronium. The formation of positronium in liquids and solids can be explained by the spur model,[75,76] in which a positron spur in the last part of the positron track is created as a result of the slowing down of the positron. In the spur, reactive species such as cations and free electrons are formed. Positronium is the result of a combination of the thermalized positron with one of the available free electrons. The formation of positronium must compete with other processes, such as electron−cation recombination, the diffusion of positrons and electrons out of the spur, and electron or positron scavenging. The o-Ps intensity $I_3$ is very sensitive to inhibition reactions taking place in the positron spur,[76,77] source exposure time,[78−81] exposure to visible light,[82] exposure to electric fields[76,83,84] and magnetic fields,[85] and the chemical structure of the materials under study.[86] This implies that changes in the o-Ps intensity $I_3$ cannot be accounted for on the basis of free volume theories. The o-Ps intensity can therefore not be considered a measure of the free volume cavity concentration.[87]

Generally, the free volume properties of glassy polymers are determined by the macromolecular conformation, thermal history, pressure, temperature, and chemical structure. Free volume properties of poly(methyl methacrylate) (PMMA) as a function of temperature and pressure history, measured in the glassy state and at temperatures above the glass transition by PALS, have been extensively studied and reported in the literature. Schmidt et al.[88−91] observed a direct correlation between the free volume fraction and the free volume cavity size for a number of pressure-densified polymer glasses, indicating the size of free volume cavities to be a controlling factor of the temperature (thermodynamic formation history, pressure densification) dependence of the specific volume. The o-Ps formation probability in glassy polymers shows large variations with temperature, thermal history, and measuring time.[80]

Several PALS studies on polymers filled with micro- or nanosized rigid fillers, such as silicas, ZnO, clay, or carbon blacks, which are introduced into polymers by directly mixing them, have been published.[65,70,92−106] In most cases, the o-Ps lifetime $\tau_3$ was not significantly affected by the presence of the different additives, which implies that thermalized Ps atoms do not react with the additives and that the change in free volume caused by the additives is rather small.[70,96] On the other hand, for the composites with the functional modification, the o-Ps lifetime decrease was observed with increasing filler concentration.[70] This was ascribed to the special interfacial interactions between the surface of nanoparticles and polymers. In addition to the mean free volume hole sizes $V(\tau_3)$, the o-Ps formation probability ($I_3$), originated from o-Ps annihilation in the polymer phase, shows a systematic decrease in systems with increasing weight fraction of inorganic fillers, which is directly related to the decrease of polymer weight fraction accessible to o-Ps.[107,108] Apart from the data of composites from the direct mixing methods, there are, to the best of our knowledge, no PALS studies of o-Ps lifetime and intensity of organic−inorganic nanocomposites and their nanohybrid fibers created by means of the in-situ sol−gel method in the literature.

In light of the recent research showing promising but not fully understood changes of properties in glassy polymers upon incorporating nonporous nanosized fillers, it is of importance to

gain deeper insight into the changes in free volume structure of these composites prepared by using the different preparation technologies, such as blending, extruding, electrospinning, or in-situ generation of hybrids using the combined method. The aim of the present study is to investigate the effect of nanosized nonporous $TiO_2$, incorporated into a PMMA matrix by simple mixing or in-situ generating, on the polymer free volume sizes and o-Ps intensity with positron annihilation lifetime spectroscopy (PALS). In addition, the thermal properties of nanohybrids were investigated by using differential scanning calorimetry (DSC).

## 2. EXPERIMENTAL METHODS

**2.1. Materials and Sample Preparation.** Poly(methyl methacrylate) (PMMA molar mass $M_w$ = 75 kg/mol, density $\rho$ = 1.20 g/cm$^3$) was obtained from Scientific Polymer Products Inc. Commercial $TiO_2$ powder (P25) with a mean diameter of 21 nm was obtained from Degussa, Germany. Tetrabutyl titanate (TBT) was purchased from Beijing Chemical Reagents Co. Trifluoroacetic acid (TFA) and dichloromethane (DCM) were used as solvent mixture (v:v = 1:1, density $\rho_{mix}$ = 1.3 g/mL). All solvents were used without further purification.

Prior to mixing, the PMMA and P25 powder were dried at 80 °C for at least 60 h under vacuum. Extruded composite samples were prepared by melt-mixing PMMA and P25 at different weight ratios in a DSM Midi 2000 corotating twin screw extruder with a chamber capacity of 15 cm$^3$, operated at 200 °C and 6 rpm for 10 min. The extruded composites and powder mixed composites with different weight ratios were compression-molded in a press at 190 °C into 2 mm thick samples. The procedure for compression molding was as following: the blends were preheated at 190 °C for 3 min and then pressed at lower pressure 1 ton for 1 min followed by pressing at a pressure of 10 ton for 2 min. The extruded samples are referred to as PM0PEB, PM2PEB, and PM4PEB. The pressed mixed powder samples are referred to as PM0PB, PM2PB, PM4PB, and so on in the following text. In addition, PMMA and P25/PMMA nanohybrid fibers were prepared by electrospinning of a TFA/DCM solution with P25 nanospheres and PMMA at different weight ratios. The samples are referred to as PM0F, PM2PF, PM4PF, PM6PF, PM8PF, and PM10PF in the following text. The actual P25 content in the nanohybrids was determined by thermogravimetric analysis (TGA) and is listed in Table 1. The fiber mats were dried at 80 °C under vacuum for 16 h to evaporate residual solvent before further pressing.

The in-situ-grown $TiO_2$/PMMA hybrid fibers were prepared as the following: The hydrolyzed TBT solution was added dropwise into the PMMA/TFA/DCM solution, followed by magnetic stirring for 1 h in an ice bath ($T$ < 10 °C). The solution containing the desired $TiO_2$ precursor content was transferred to a glass syringe capped with a 9-gauge blunt end needle for electrospinning. As a result of the high voltage applied, the $TiO_2$ precursor/PMMA hybrid fibers were collected on the grounded aluminum foil and are designated as PM8F, PM15F, PM20F, PM25F, and PM30F in the following text. After spinning, the titania precursor/PMMA fiber mats were dried for 2 days under vacuum at 30 °C to allow the residual solvent to evaporate before post-treatment for in-situ formation of $TiO_2$. Afterward, the nanohybrid fiber mats were treated in a hot water container at different temperatures (70, 80, 90, and 100 °C) for 24 h. All the samples were subsequently washed by using distilled water and dried at 70 °C for 3 h. The exact compositions of in-situ grown $TiO_2$/PMMA nanohybrid fibers were deduced from TGA measurements and are listed in Table 1.

All the fiber mats samples used for the PALS measurements were cut in two equal parts and were folded into 2 × 2 cm pieces each and pressed into 2−3 mm thick samples at room temperature for 1 min at 5 ton. Two equal samples are necessary for one PALS measurement.

**2.2. DSC Measurements.** The thermal properties of the materials were studied using a DSC Q1000 from TA Instruments during a second scan. The samples of 2−3 mg were contained in aluminum pans, and the analysis was performed from 30 to 170 °C at a heating rate of 20 °C/min under nitrogen purge with the flow rate of 50 mL/min. The first scan was run to 170 °C to erase previous thermal history, and then the samples were cooled to 30 °C at a cooling rate of 20 °C/min to start the second scan.

**2.3. Thermogravimetric Analysis.** The components of hybrid materials were evaluated using a TGA Q500 from TA Instruments with a heating rate of 20 °C/min under a nitrogen flow rate of 60 mL/min. The sample weight was 3−4 mg for TGA measurements. The actual inorganic P25 filler content in the composites was determined by the residue content in the TGA scan. The total content of hydroxyl groups in the precursor/PMMA composite fibers was deduced from the weight loss between 100 and 295 °C and above 420 °C. However, for the $TiO_2$/PMMA hybrid fibers produced by the in-situ method, the content of unreacted hydroxyl groups was calculated from the weight loss above 420 °C and the last residue content was the actual formed $TiO_2$ concentration.[56]

**2.4. Positron Annihilation Lifetime Spectroscopy.** All PALS measurements were performed at 23 °C using a fast−fast coincidence system. The two identical $\gamma$-ray detectors, placed at ∼160° to each other and at least 2.5 cm apart to minimize backscattering, consist of CsF crystals mounted on Hamamatsu photomultiplier tubes. The samples were placed in a sandwich configuration with a sodium 22 radioactive source contained in Kapton foils. Samples used were pressed plates or nanohybrid fiber mats, pressed with the procedure as described above.

Five positron lifetime spectra, each containing 2.3 million counts, were collected for each sample at 23 °C and evaluated with PALSFIT 1.54 software using no source correction and one fixed lifetime of 260 ps. This evaluation method extracts lifetime and intensity values from the spectra with a model function consisting of a sum of decaying exponentials convoluted with the resolution function of the lifetime spectrometer plus a constant background. All spectra were evaluated using three lifetimes. Trials to fit the spectra with four lifetimes were unsuccessful. The PALS measurements were all performed within 4−8 weeks after the preparation of the samples.

## 3. THEORETICAL BACKGROUND: FORMATION OF $TIO_2$ IN ELECTROSPUN PMMA FIBERS VIA AN IN-SITU SOL−GEL METHOD

Sol−gel processing provides for excellent chemical homogeneity and the possibility of deriving unique metastable structures at low reaction temperatures. It involves the hydrolysis and condensation reactions of molecular precursors such as metal alkoxides or metal salts as shown in the following:

hydrolysis:

$$\mathrm{Ti{-}OR + H_2O \rightarrow Ti{-}OH + R{-}OH}$$

condensation :

$$\mathrm{Ti{-}OH + Ti{-}OR \rightarrow Ti{-}O{-}Ti + R{-}OH}$$

$$\mathrm{Ti{-}OH + Ti{-}OH \rightarrow Ti{-}O{-}Ti + H_2O}$$

$$\mathrm{R = organic\ group}$$

The relative rates of hydrolysis and condensation strongly influence the structure and properties of the resulting metal oxides. Factors affecting the sol−gel process include the reactivity of metal alkoxides, pH of the reaction medium, water:alkoxide ratio, reaction temperature, and nature of solvent and additives.[109,110]

**Table 1. Composition and Properties of the Prepared Materials**

| sample | $T_H$[a] (°C) | $C_{-OH}$[b] (wt %) | $C_{TiO2}$[b] (wt %) | $\tau_3$ (ns) | $I_3$ (%) | $T_g$ (°C) |
|---|---|---|---|---|---|---|
| PM0F | | 0 | 0 | 1.87 | 25.0 | 109.2 |
| PM8F | | 13.6 | 0 | 1.84 | 15.0 | 118.2 |
| PM15F | | 17.8 | 0 | 1.77 | 10.4 | 120.1 |
| PM20F | | 22.3 | 0 | 1.68 | 9.3 | 123.6 |
| PM25F | | 25.2 | 0 | 1.65 | 7.7 | 127.3 |
| PM30F | | 27.0 | 0 | 1.55 | 6.3 | 135.1 |
| PM0-70F | 70 | 0 | 0 | 1.90 | 25.0 | 109.2 |
| PM8-70F | 70 | 3.1 | 3.4 | 1.85 | 17.3 | 116.5 |
| PM15-70F | 70 | 5.7 | 4.9 | 1.83 | 14.9 | 117.3 |
| PM20-70F | 70 | 6.4 | 6.2 | 1.81 | 13.6 | 119.2 |
| PM25-70F | 70 | 6.3 | 8.8 | 1.83 | 12.9 | 120.0 |
| PM30-70F | 70 | 7.4 | 9.7 | 1.79 | 12.5 | 120.7 |
| PM0-80F | 80 | 0 | 0 | 1.91 | 25.0 | 109.1 |
| PM8-80F | 80 | 2.8 | 2.6 | 1.88 | 18.8 | 114.0 |
| PM15-80F | 80 | 4.0 | 4.9 | 1.86 | 17.1 | 114.2 |
| PM20-80F | 80 | 4.3 | 6.1 | 1.84 | 16.2 | 116.4 |
| PM25-80F | 80 | 5.2 | 7.8 | 1.83 | 15.7 | 116.4 |
| PM30-80F | 80 | 5.7 | 9.5 | 1.85 | 14.8 | 118.5 |
| PM0-90F | 90 | 0 | 0 | 1.91 | 24.7 | 110.5 |
| PM8-90F | 90 | 1.9 | 2.3 | 1.91 | 21.2 | 112.2 |
| PM15-90F | 90 | 2.3 | 4.5 | 1.90 | 20.2 | 113.7 |
| PM20-90F | 90 | 2.3 | 6.0 | 1.89 | 19.8 | 114.6 |
| PM25-90F | 90 | 2.7 | 7.7 | 1.87 | 19.0 | 114.6 |
| PM30-90F | 90 | 2.4 | 9.6 | 1.89 | 18.6 | 114.8 |
| PM0-100F | 100 | 0 | 0 | 1.92 | 23.0 | 110.6 |
| PM8-100F | 100 | 0.9 | 2.4 | 1.92 | 22.9 | 111.9 |
| PM15-100F | 100 | 0.9 | 4.1 | 1.91 | 21.8 | 112.8 |
| PM20-100F | 100 | 1.8 | 6.0 | 1.88 | 21.5 | 113.2 |
| PM25-100F | 100 | 2.1 | 7.5 | 1.91 | 20.6 | 113.3 |
| PM30-100F | 100 | 2.3 | 9.2 | 1.89 | 20.6 | 113.3 |
| $TiO_2$ precursor | | 52.0[c] | 39.0[c] | | 0 | |
| PM2PF | | 0 | 2.8 | 1.88 | 24.0 | 110.6 |
| PM4PF | | 0 | 4.6 | 1.88 | 22.4 | 109.0 |
| PM6PF | | 0 | 6.2 | 1.87 | 23.4 | 109.5 |
| PM8PF | | 0 | 8.5 | 1.88 | 23.1 | 111.4 |
| PM10PF | | 0 | 9.7 | 1.87 | 22.2 | 110.5 |
| PM0PB | | 0 | 0 | 1.87 | 25.2 | 111.2 |
| PM2PB | | 0 | 2.1 | 1.87 | 24.6 | 110.0 |
| PM4PB | | 0 | 3.1 | 1.86 | 24.2 | 109.7 |
| PM6PB | | 0 | 4.0 | 1.86 | 24.0 | 111.2 |
| PM8PB | | 0 | 5.9 | 1.86 | 23.6 | 111.0 |
| PM10PB | | 0 | 7.1 | 1.86 | 23.3 | 112.0 |
| PM0PEB | | 0 | 0 | 1.88 | 25.2 | 109.2 |
| PM2PEB | | 0 | 2.6 | 1.88 | 24.9 | 109.0 |
| PM4PEB | | 0 | 4.5 | 1.87 | 24.6 | 109.7 |

[a] Temperature of hydrothermal treatment. [b] Contents from TGA results. [c] Experimental content on the assumption that the precursor has fully reacted under TGA scan in nitrogen.

By varying these processing parameters, materials with different microstructure and surface chemistry can be obtained. In the case of polymer matrices, the final structure of the inorganic network and morphology of the composite are further influenced by the relative rates of vitrification and the rate of inorganic network formation.[111,112]

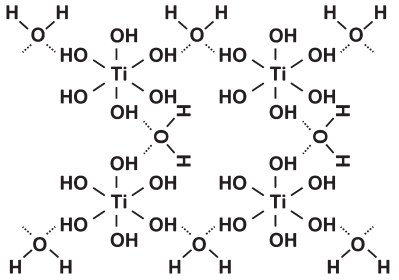

**Figure 1.** Structure of hydrolyzed titania precursor of $Ti(OH)_6 \cdot 2H_2O$.

In the preparation of nanosized $TiO_2$/PMMA hybrid fibers by using electrospinning combined with the sol−gel method, the hydrolysis of TBT in a solvent mixture of TFA and DCM was accelerated by acid TFA to form a relatively stable titania precursor solution, in which the condensation reaction would be intentionally delayed. The structure $Ti(OH)_6 \cdot 2H_2O$ of the titania precursor has been verified by FTIR and TGA measurements,[56] in which the hydrolyzed $Ti(OH)_6$ was the basic unit containing six hydroxyl groups in each unit, which can be linked by molecular water as hydrogen-bonding interaction. This results in the formation of the inorganic precursor network, as illustrated in Figure 1. After incorporating the inorganic precursor solution into the PMMA solution, followed by fast electrospinning to produce the stable titania precursor/PMMA fibers, the condensation of prehydrolyzed precursor could be retarded by the fast evaporation of solvent in this process. In addition, the homogeneous dispersion of the precursor in the composite fibers has been facilitated due to the rapid vitrification of PMMA in the electrospinning process. Importantly, the interaction between the hydroxyl groups in $TiO_2$ precursor and carbonyl groups in PMMA matrix by forming the strong hydrogen bonds contributes to the stability of precursor in the polymer fiber matrices as proved by FTIR analysis.[56] Subsequently, the mild hydrothermal treatment in the temperature range from 70 to 100 °C induces the in-situ formation of $TiO_2$ nanoparticles, in which condensation of the precursor initiates a loss of a large amount of hydroxyl groups. It is worth noting that the one-dimensional fiber structure of the polymer provides a practical tool for inducing the homogeneous formation of $TiO_2$ nanoparticles with a mean diameter of 5 nm in the PMMA matrix during the postsynthesis treatment in hot water. The mild neutral hydrothermal treatment below the glass transition temperature ($T_g$) of PMMA prevented the decomposition of the polymer matrix. Furthermore, the phase separation of organic and inorganic constituents has been restrained through the hydrogen-bonding interaction between residual hydroxyl groups on the surface of in-situ-grown titania and carbonyl groups in PMMA.

## 4. RESULTS AND DISCUSSION

**4.1. Free Volume Properties of PMMA Hybrids Filled with P25 Particles.** Figure 2 shows the o-Ps lifetime in P25 filled PMMA composites as a function of filler content, which were prepared by means of the extruding, blending, and electrospinning of P25/PMMA mixtures. The mean o-Ps lifetime in PMMA is about 1.88 ns and does not show any significant dependence on filler content

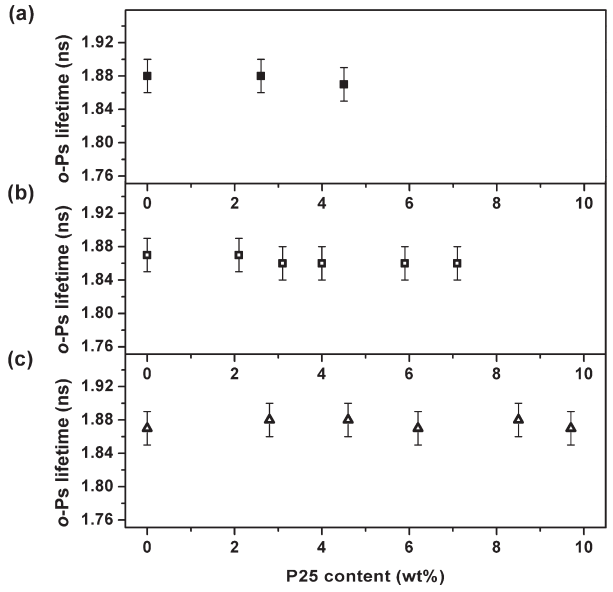


**Figure 2.** o-Ps lifetime in P25/PMMA nanohybrids at 23 °C as a function of P25 content: (a) extruded discs, (b) blended discs, and (c) pressed electrospun fibers.

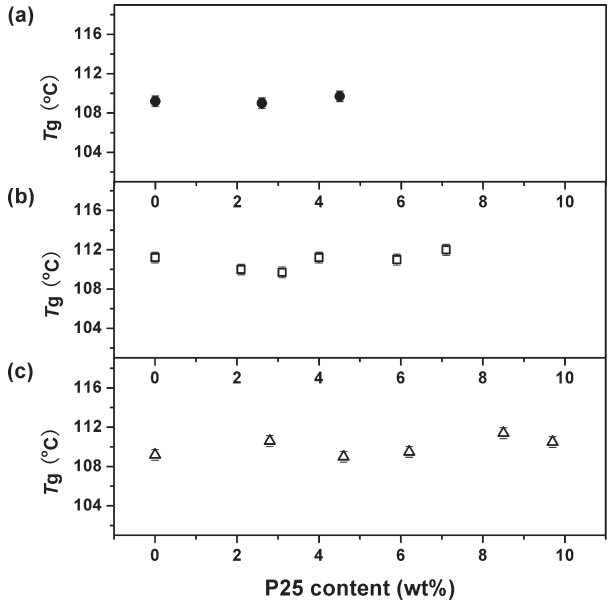


**Figure 3.** Glass transition temperature in P25/PMMA nanohybrids as a function of P25 content measured by DSC: (a) extruded discs, (b) blended discs, and (c) pressed electrospun fibers.

within the accuracy of the experiment for all samples prepared by the different mixing methods. Meanwhile, no o-Ps lifetime was observed in pure P25 nanoparticles, which shows that inorganic particles would not contribute to the o-Ps lifetime in the PALS spectrum. These results are ascribed to the absence of a functional interface between P25 particles and the polymer matrix. As shown in Table 1, the P25 particles have a negligible number of surface hydroxyl groups available for interaction, which does not lead to any observable change in free volume cavity size of the PMMA matrix.

Additionally, the glass transition temperatures ($T_g$) of the composites were investigated by DSC. Figure 3 shows the glass transition

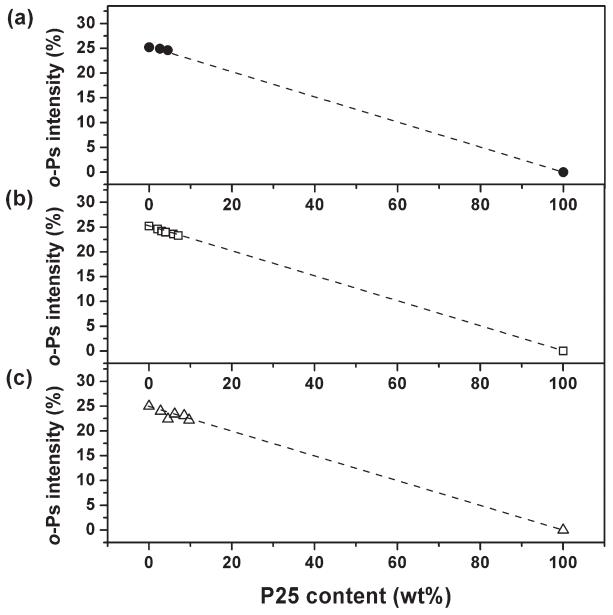


**Figure 4.** Intensities of o-Ps formation in P25/PMMA nanohybrids at 23 °C as a function of P25 content: (a) extruded discs, (b) blended discs, and (c) pressed electrospun fibers. Dotted lines represent the predictions according to eq 2b based on the experimental annihiliation data of PMMA and P25.

temperatures ($T_g$) of P25 filled composites as a function of filler content. The $T_g$'s of the nanosized P25 filled PMMA composites are independent of filler loading for all three processing procedures.

Figure 4 displays the o-Ps intensities in PMMA/P25 composites corresponding to the formation probability of o-Ps in the free volume cavities of the samples prepared by using the extruding, blending, and electrospinning methods. For the different preparation methods, the pressed PMMA fibers have about 1% lower intensity values of $I_3$ in comparison to the blended and extruded samples. The reason may be that there is still a minor content of larger empty voids in the pressed fiber samples which reduce slightly the amount of matrix material accessible for the positrons. By mixing of P25 nanoparticles to PMMA, the measured decrease of the o-Ps intensity with increasing content of nanosized P25 is clearly observed. This behavior of $I_3$ is in accordance with eq 2a. A linear relationship exists between the weight fraction of the constituents and the total o-Ps, p-Ps, and free positron intensity for conventional polymer composites with micrometer-sized filler particles and polymer blends with micrometer-sized grains,[107,108] where c, p, and m indicate composite, particle, and matrix, respectively.

$$I_{3c} = w_p I_{3p} + (1 - w_p) I_{3m} \quad (2a)$$

In this study, we simultaneously investigated the o-Ps formation in pure P25 nanoparticles at 100% filler content. No long o-Ps lifetime was detectable. As a result, the linear relationship between the weight fraction of the constituents and the o-Ps intensity in P25 filled PMMA composites can be represented by eq 2b

$$I_3 = I_3^0 (1 - w_p) \quad (2b)$$

**4.2. Free Volume Properties of $TiO_2$ Precursor/PMMA Nanocomposite Fibers.** Figure 5 shows the o-Ps lifetime in $TiO_2$ precursor/PMMA composite fibers as a function of hydroxyl group content. The o-Ps lifetime reduces with increasing the −OH

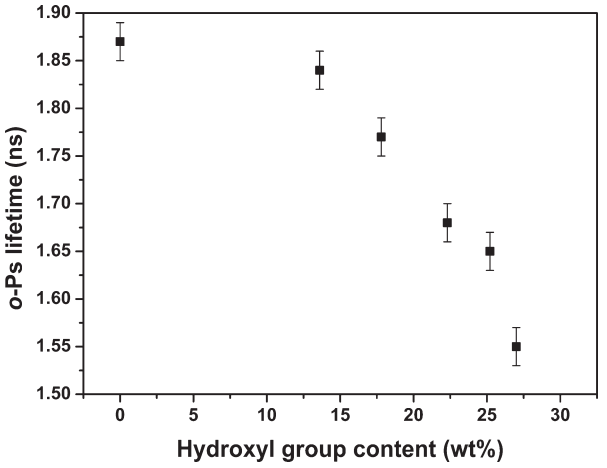


**Figure 5.** o-Ps lifetime in titania precursor/PMMA composite fibers at 23 °C as a function of hydroxyl group content.

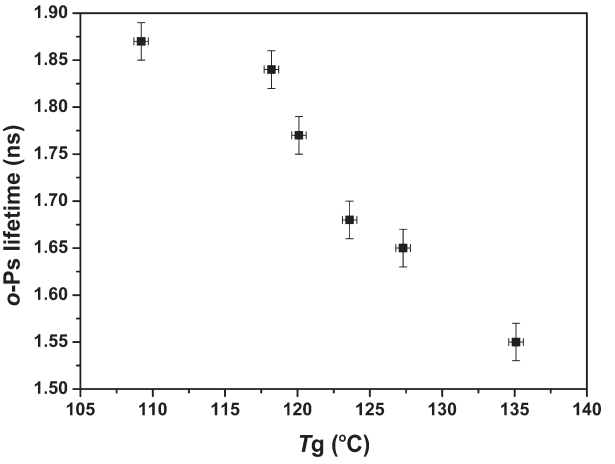


**Figure 6.** Relation between the glass transition temperature of titania precursor/PMMA composite fibers and the o-Ps lifetime.

content from 1.87 ns in pure PMMA fibers to 1.55 ns in PM30F, in which the hydroxyl group content increased to about 27.0 wt % as shown in Table 1. This observation indicates that the o-Ps lifetime and free volume cavity size are strongly dependent on the weight fraction of hydroxyl groups in the titania precursor/PMMA nanocomposite fibers. The decrease in free volume can be explained by the interfacial interaction between the constituents. Previous research has established the existence of strong hydrogen-bonding interactions between the hydroxyl groups in $Ti(OH)_6 \cdot 2H_2O$ precursor and the carbonyl groups in PMMA chains.[56] Moreover, the effect of interfacial interaction was strengthened by the increasing amount of hydroxyl groups in precursor/PMMA composite fibers. This increased interaction, unlike the P25/PMMA composites, reduces the mobility of the polymer segments. A similar decrease in o-Ps lifetime can be observed by hydrogen bonding in the amorphous phase of polyamides as a function of amide content.[78]

Such diminished free volume size originated from the molecular interaction between inorganic moiety and the polymer matrix molecules can be expected to strongly affect the physical properties of the resulting composites. It is therefore, also from an application point of view, of great interest to investigate the thermal properties of the titania precursor/PMMA composite fibers.

Figure 6 shows the relation between the glass transition temperatures in titania precursor/PMMA composite fibers and the o-Ps lifetime in precursor filled and unfilled fibers, respectively. The pure PMMA fibers exhibit a $T_g$ value around 109 °C. Significantly, all the precursor composite fibers show an increased $T_g$ compared to pure PMMA, from 118.2 °C in PM8F to 135.1 °C in PM30F. It confirms the existence of strong molecular interactions between the precursor and PMMA which affects both $T_g$ and o-Ps lifetime.

Figure 7 shows the o-Ps intensity in titania precursor/PMMA composite fibers as a function of hydroxyl group content. The $I_3$ value of pure PMMA fibers is close to 25.0%, but the o-Ps yield decreases dramatically with increasing amount of hydroxyl groups in the precursor/PMMA composites. o-Ps formation was additionally not found in the pure precursor indicated as a 100% filler content as shown in Table 1. The large negative change in $I_3$ shows that the o-Ps yield is strongly dependent on the hydroxyl group content, which appears to inhibit Ps formation. From what is known earlier, a marked reduction in the o-Ps intensity would be expected owing to the stronger inhibiting effects caused by the presence of a larger number of high electron affinity groups as an electron acceptor, like nitro and halogen, which can reduce electron availability and positronium yield.[71,108,113] Herein, the hydroxyl group acts as electron scavenger, whereas PMMA has a much lower probability of recombining with free electrons, which can be demonstrated by the high o-Ps intensity (~25.0%) in pure PMMA. This means that Ps formation is strongly inhibited in the parts of the spur where −OH is situated, whereas the Ps formation probability is much higher in the PMMA-rich parts of the spur. The o-Ps formation probability will then obviously depend on the concentration of the electron-scavenging groups, which in this case are represented by the concentration of hydroxyl groups. An equation describing the decrease in $I_3$ with increasing −OH concentration is proposed here as follows:

$$I_3 = I_3^0\left[\frac{1+A}{1+C} - A\right] \tag{3}$$

where $C$ is the concentration of scavenger hydroxyl group in units of weight concentration, $I_3^0$ is the o-Ps yield at $C = 0$, and $A$ is a constant related to the inhibition efficiency of hydroxyl groups. The best-fit values of $I_3^0$ and $A$ as well as the lowest concentration of hydroxyl group inducing zero o-Ps formation, given as $1/A$, are listed in Table 2. It is seen that the hydroxyl groups completely inhibit Ps formation when its concentration attains 39.8 wt % in the precursor/PMMA nanocomposites.

**4.3. Free Volume Properties of in-Situ Grown $TiO_2$/PMMA Hybrid Fibers.** Figure 8 shows the o-Ps lifetimes of in-situ-grown $TiO_2$/PMMA nanohybrid fibers as a function of treatment temperature in water. The pure PMMA fibers exhibit a slightly increased o-Ps lifetime with increasing treatment temperature from 70 to 100 °C. Figure 8 shows strong effects dependent on the treatment temperature, for example, a large increase of o-Ps lifetime was observed in PM30-70F to 1.79 ns, compared to 1.55 ns in the untreated PM30F as shown in Table 1. Subsequently, with increasing the hydrothermal treatment temperature, the lifetime of o-Ps increases significantly and systematically from 1.79 ns in PM30-70F to 1.89 ns in PM30-100F, which is 0.03 ns shorter than PM0-100F and close to the original lifetime of unfilled PMMA treated at 100 °C hot water. The similar tendency was observed in other precursor/PMMA fibers samples

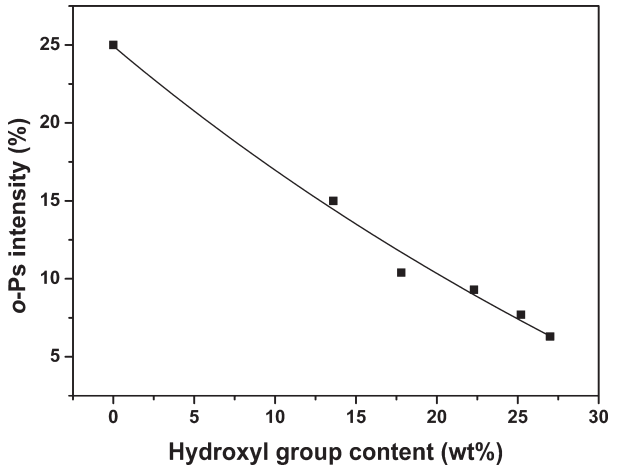


**Figure 7.** Intensities of o-Ps formation in titania precursor/PMMA composite fibers 23 °C as a function of hydroxyl group content. Solid line represents the best fit of eq 3 to experimental data.

**Table 2. Best-Fit Values of $I_3^0$ and $A$ in eq 2b and the Lowest Value of $C$ When $I_3 = 0$**

| sample | $I_3^0$ (%) | $A$ | $C_0$ (wt %) |
|---|---|---|---|
| precursor/PMMA fibers | 24.9 | 1/0.398 | 39.8 |
| in-situ-formed $TiO_2$/PMMA fibers | 24.0 | 1/0.157 | 15.7 |

as well, which were all treated in hot water in the range 70−100 °C. These results illustrate that the treatment temperature has an influence on the free volume cavity size of the PMMA in the composites. In addition, Figure 9 shows the residual hydroxyl group content as a function of treatment temperature. For every series of samples, a decrease of the amount of unreacted hydroxyl groups was observed with increasing the treatment temperature from 70 to 100 °C, comparing with the untreated precursor/PMMA composite fibers. Contrary to the decrease of o-Ps lifetime in precursor/PMMA fibers due to the strong interaction of PMMA matrix with the precursor by forming the hydrogen bonds, a lower probability for interactions between the unreacted hydroxyl groups on the surface of the grown $TiO_2$ and PMMA matrix can be expected as the amount of −OH decreased in the composite fibers. These findings encourage the further exploration of a correlation between thermal properties and o-Ps lifetime (free volume cavity size) in $TiO_2$/PMMA hybrid fibers generated by the in-situ method.

Figure 10 illustrates the dependence of $T_g$ on o-Ps lifetime in composites with different treating conditions. Interestingly, for example, the decrease of $T_g$ was observed at 120.7 °C in PM30-70F compared with 135.1 °C in untreated PM30F; accordingly, the o-Ps lifetime was increased from 1.55 to 1.79 ns. A significant decrease after treatment was believed to result from the increment of free volume in polymer, which makes it easier for the mobility of polymer segments. Further decrease of $T_g$ was substantially observed to 113.3 °C in PM30-100F, in which o-Ps lifetime increased to 1.89 ns. For this particular system, treating the sample at elevated temperatures for a sufficient amount of time induces to the recovery of free volume cavity size in composites and leads to a value of $T_g$ which approaches the $T_g$ of pure PMMA treated at the same condition. Similar phenomena were observed for the other samples as well. These

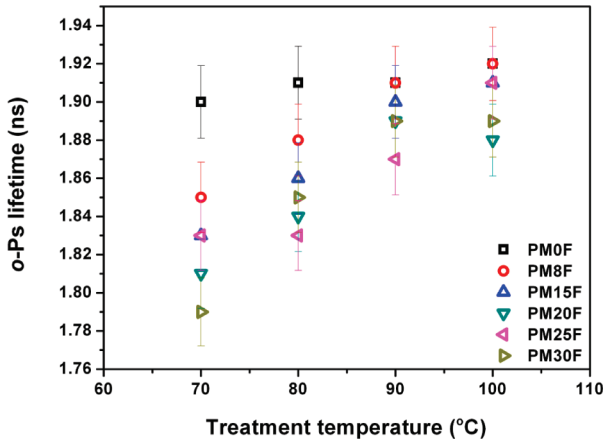


**Figure 8.** o-Ps lifetime in $TiO_2$/PMMA hybrid fibers at room at 23 °C as a function of treatment temperature.

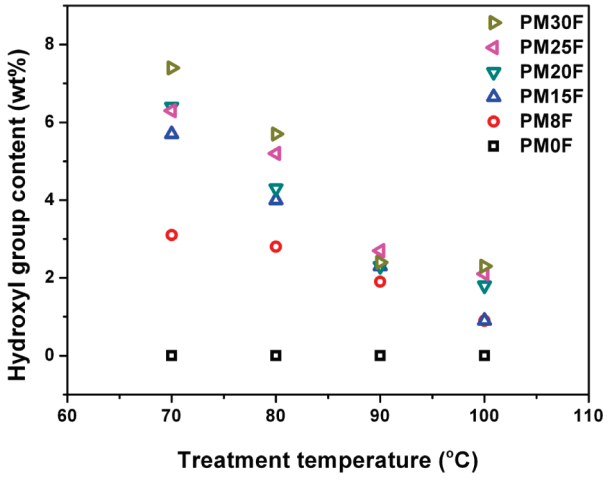


**Figure 9.** Content of unreacted hydroxyl groups in in-situ-grown $TiO_2$/PMMA hybrid fibers as a function of treatment temperature measured by TGA.

results confirm a strong interaction between the polymer and titania surfaces by in-situ methods for the samples treated at lower temperatures, where the concentration of residual hydroxyl groups acting as physical cross-links is higher than that treated at higher temperatures.

Figure 11 shows the intensity of o-Ps formation in $TiO_2$/PMMA nanohybrid fibers as a function of treatment temperature. Interestingly, for example, $I_3$ was increased from 6.3% in PM30F to 12.5% in PM30-70F. The significant and linear increment was observed as increasing the treatment temperature from 70 to 100 °C. Similarly, a consecutive increment of $I_3$ was observed for other series of samples, which were treated at the elevated temperature as well. It is interesting to note that, in the samples treated in hot water at 100 °C for 24 h, the intensity of o-Ps formation in the nanohybrid fibers with different weight fraction of in-situ-generated $TiO_2$ was very close to the $I_3$ value in PMMA filled with inorganic $TiO_2$ calculated by using eq 2b. For the in-situ generation, it means the full conversion of precursor into the $TiO_2$ is independent of the amount of precursor present under hydrothermal treatment, which can be assumed to be reached at the maximum treatment temperature $T_{max}$, equal or


dx.doi.org/10.1021/ma201004b |*Macromolecules* 2011, 44, 5711–5721

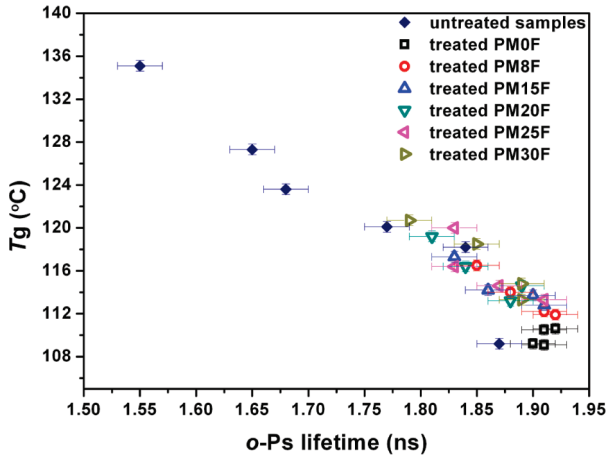


**Figure 10.** Relation between the glass transition temperature of in-situ-grown $TiO_2$/PMMA hybrid fibers and the o-Ps lifetime before and after the different temperature treatments.

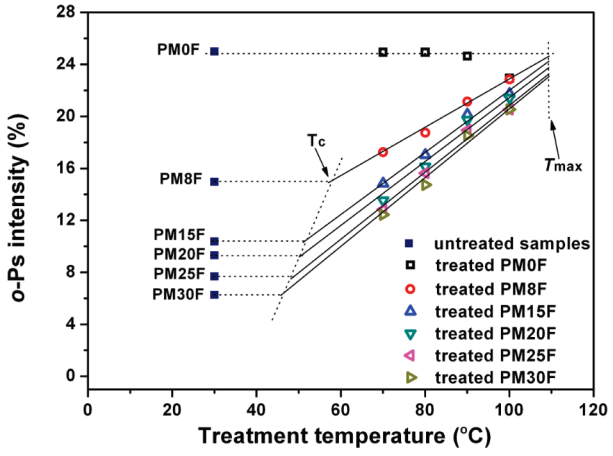


**Figure 11.** Intensities of o-Ps formation in in-situ-grown $TiO_2$/PMMA hybrid fibers at 23 °C as a function of treatment temperature. Solid lines represent the predictions according to eq 4.

close to the glass transition temperature ($T_g$) of PMMA. On the basis of above analysis, a linear relationship between the intensity of o-Ps formation and the treatment temperature could be fitted as follows:

$$I_{3c} = I_3^0(1 - w_{p,Tmax})[1 - (T_{max} - T)/(T_{max} - T_0)] \quad (4)$$

$I_3^0$ is the o-Ps yield in pure PMMA, $w_{p,Tmax}$ is the weight content of inorganic fillers under the full conversion at the treatment temperature $T_{max}$, $T_{max}$ is the maximum treatment temperature where all precursor is transferred into $TiO_2$ without the unreacted −OH, and $T_0$ is a fictive temperature, where $I_3$ is zero. Equation 4 is valid only for intensity > $I_3$ at $T_c$. $I_3$ at $T_c$ is a function of −OH concentration in precursor/PMMA composites as described in eq 3, where $T_c$ is a critical temperature, only above which the condensation of precursor could start. The best-fit values of $w_{p,Tmax}$, $T_0$, and $T_c$ are listed in Table 3.

It has been shown that the treatment temperature can influence the dehydration of hydroxyl groups of the precursor, considering that the inorganic fillers have a negative linear influence on $I_3$ in composites and that the effect of hydroxyl

**Table 3. Best-Fit Values of $w_{p,Tmax}$, $T_0$ and $T_c$ in eq 3**

| sample | $w_{p,Tmax}$ (wt %) | $T_0$ (°C) | $T_c$ (°C) |
|---|---|---|---|
| PM8F | 1.48 | −28.03 | 57.95 |
| PM15F | 2.76 | 4.84 | 51.52 |
| PM20F | 4.48 | 8.63 | 50.21 |
| PM25F | 7.00 | 16.59 | 47.93 |
| PM30F | 8.24 | 19.51 | 45.98 |

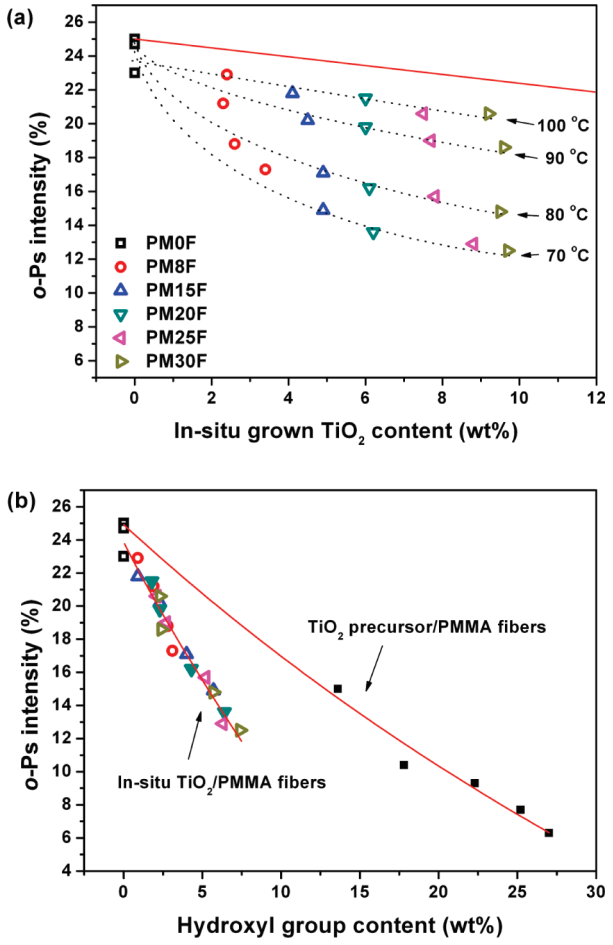


**Figure 12.** Intensities of o-Ps formation in $TiO_2$/PMMA nanohybrid fibers at room temperature as a function of in-situ-formed $TiO_2$ content (a) and as a function of unreacted hydroxyl group content (b). Symbols represent experimental data, solid lines represent the predictions according to eq 2b (a) and eq 3 (b), and dotted lines represent the isothermal lines of treatment temperature.

groups on $I_3$ has been observed in the precursor composites as well. It is of interest to investigate the effects of in-situ-grown $TiO_2$ and residual hydroxyl groups on the $I_3$ in the in-situ-generated $TiO_2$/PMMA nanohybrids. Figure 12a displays the experimental o-Ps intensity and theoretical intensity estimated with eq 2b for in-situ-generated $TiO_2$/PMMA fibers as a function of nanosized titania content. In the case of nanosized titania generation in PMMA, $I_3$ decreased with increasing $TiO_2$ content at the same treatment conditions but does not follow the linear weight averaging relationship (eq 2b). A negative deviation between the experimental o-Ps intensity and the theoretical

o-Ps intensity is present, although the experimental lines were gradually close to the theoretical prediction with increasing the treatment temperature. It appears that the o-Ps formation in the polymer is extensively decreased when nanosized titania is formed by means of the in-situ method, in comparison with PMMA filled with P25 nanospheres. It has been shown that the unreacted hydroxyl groups remain on the surface of the in-situ-formed $TiO_2$. Moreover, the truth verified that the inhibition effect of hydroxyl groups on the formation probability of o-Ps in polymer. On the basis of above analysis, it is possible that the deviation of $I_3$ is caused by the presence of residual hydroxyl groups in nanohybrid fibers.

The experimental o-Ps intensity for hybrid fibers as a function of residual hydroxyl group content is shown in Figure 12b. It can be observed that the $I_3$ values of all the hybrid fibers containing unreacted hydroxyl groups are clearly lower than that of pure PMMA fibers. The effect of hydroxyl groups could be explained by using the similar mechanism as in precursor/PMMA composite fibers. In addition to the conventional linear reduction of intensity by inorganic fillers as has been reported, the residual hydroxyl groups in the composite fibers remain as electron scavenger to inhibit the formation of o-Ps as illustrated in the precursor/PMMA fibers. The measured o-Ps intensity with increasing content of unreacted hydroxyl groups was reduced and can be fitted to a linear relationship represented by eq 3, which had been observed in PMMA nanocomposite fibers containing the precursor $Ti(OH)_6 \cdot 2H_2O$. Herein, the best-fit values of $I_3^0$ and $A$ are listed in Table 2. It is found that the $I_3^0$ of 24.0% in in-situ $TiO_2$/PMMA fibers is slightly lower than the $I_3^0$ with 24.9% in the precursor composite fibers. This result can be explained by the in-situ-formed $TiO_2$ effect on the composites, in which $I_3^0$ is actually the intensity of o-Ps in PMMA hybrids filled with in-situ $TiO_2$ nanoparticles with the content in the range from 0 to 10 wt % under the situation of the full conversion of precursor without unreacted −OH. Meanwhile, it is also clear that the value of $A$ in in-situ $TiO_2$/PMMA nanohybrids is higher than its value in precursor/PMMA nanocomposites. As mentioned earlier, $A$ represents the inhibition efficiency of hydroxyl groups on the Ps formation. This result shows a stronger inhibition effect of −OH in in-situ $TiO_2$/PMMA nanohybrids than in precursor/PMMA nanocomposites. For the $TiO_2$/PMMA hybrid fibers prepared by the in-situ method, in fact, the large effect on $I_3$ could be explained by considering that the unreacted hydroxyl groups were mainly located at the surface of the in-situ-formed $TiO_2$. This increases the probability of interaction of hydroxyl groups with the polymer segments compared to the hydroxyl groups which are located in the precursor clusters in precursor/PMMA composite fibers. As a result, the stronger inhibition effect of −OH in in-situ $TiO_2$/PMMA hybrid fibers can be found with the same content of hydroxyl groups. This would explain the value of 15.7 wt % of hydroxyl group content, which induced zero o-Ps yield in in-situ $TiO_2$/PMMA fibers, is appreciable lower than the value of 39.8 wt % in the precursor/PMMA fibers.

## 5. CONCLUSIONS

The o-Ps lifetime in composites filled with P25 nanoparticles was constant, whereas a strong decrease was observed in the titania precursor/PMMA composite fibers, in which a large amount of hydroxyl groups present in titania precursor could form strong hydrogen-bonding interaction with the carbonyl groups in the PMMA matrix, leading to shorter intersegmental distances between the polymer chains. DSC results showed a substantial increase of glass transition temperature when the titania precursor was added.

A linear dependence of $I_3$ with inorganic filler content was observed for P25 filled nanocomposites. For the titania precursor/PMMA composites, the o-Ps intensity $I_3$ exhibits a significant linear decrease with increasing hydroxyl group content, which is interpreted as a strong inhibition effect of the hydroxyl groups on the o-Ps formation. This effect is probably related to electron or positron scavenging in the positron spur.

However, the situation is changed after hydrothermal treatment for 24 h, which facilitates the formation of $TiO_2$. TGA results showed a decreased hydroxyl group content as the treatment temperature increased, and a reduced interaction between inorganic and organic segments, thus resulting in an increase of o-Ps lifetime, o-Ps intensity, and a decrease in glass transition temperature. A linear relationship between $I_3$ and treatment temperature below $T_g$ was also observed.

The reduction of o-Ps intensity due to the formation of $TiO_2$, however, in the case of the nanosized $TiO_2$ particles/PMMA hybrid fibers, does not follow a linear relationship with filler content, which was observed for the P25 fillers. It can be explained by the presence of unreacted hydroxyl groups in $TiO_2$/PMMA hybrid fibers. Moreover, since the residual hydroxyl groups were mainly located at the surface of the formed $TiO_2$, it can more easier interact with the polymer matrix, as electron scavenger, inducing to the higher inhibition efficiency on the o-Ps formation compared to the hydroxyl groups in titania precursor/PMMA fibers.

## AUTHOR INFORMATION

### Corresponding Author

*Fax +46 46 222 4012, Tel +46 46 222 9149, e-mail frans.maurer@polymat.lth.se (F.H.J.M.); Fax +86 10 8261 5665, Tel +86 10 8261 5665, e-mail yms@iccas.ac.cn (M.Y.).

## ACKNOWLEDGMENT

The authors thank Elin Persson Jutemar for the help in the preparation of extruded samples. We acknowledge the financial support of the Swedish Research Council, the National Natural Science Foundation of China (50973115), and the Major Basic Research Projects of China (2010CB933500).

## REFERENCES

(1) Chatterjee, A. *J. Appl. Polym. Sci.* **2010**, *116*, 3396–3407.
(2) Smaihi, M.; Jermoumi, T.; Marigan, J.; Noble, R. D. *J. Membr. Sci.* **1996**, *116*, 211–220.
(3) Liou, G. S.; Lin, P. H.; Yen, H. J.; Yu, Y. Y.; Chen, W. C. *J. Polym. Sci., Part A: Polym. Chem.* **2010**, *48*, 1433–1440.
(4) Fu, T. Z.; Yu, L. X.; Wang, Z.; Yu, W. Z.; Zhao, C. J.; Zhong, S. L.; Cui, J. W.; Shao, K.; Na, H. *Polym. Compos.* **2009**, *30*, 948–954.
(5) Yang, Y. N.; Wang, P. *Polymer* **2006**, *47*, 2683–2688.
(6) Nazir, T.; Afzal, A.; Siddiqi, H. M.; Ahmad, Z.; Dumon, M. *Prog. Org. Coat.* **2010**, *69*, 100–106.
(7) Bershtein, V. A.; Gun'ko, V. M.; Karabanova, L. V.; Sukhanova, T. E.; Yakushev, P. N.; Egorova, L. M.; Glievyy, O. B.; Lutsyk, E. D.; Pakhlov, E. M.; Turova, A. A.; Zarko, V. I.; Vylegzhanina, M. E. *J. Macromol. Sci., Part B: Phys.* **2010**, *49*, 18–32.
(8) Karaman, M.; Kooi, S. E.; Gleason, K. K. *Chem. Mater.* **2008**, *20*, 2262–2267.

(9) De Sitter, K.; Winberg, P.; D'Haen, J.; Dotremont, C.; Leysen, R.; Martens, J. A.; Mullens, S.; Maurer, F. H. J.; Vankelecom, I. F. J. *J. Membr. Sci.* **2006**, *278*, 83–91.
(10) Liu, Y. H.; Chang, M. C.; Liu, P. I.; Chung, L. C.; Shao, H.; Huang, M. S.; Horng, R. Y.; Yang, A. C. M. *J. Mater. Sci.* **2010**, *45*, 6212–6217.
(11) Kuan, H. C.; Chiu, S. L.; Chen, C. H.; Kua, C. F.; Chiang, C. L. *J. Appl. Polym. Sci.* **2009**, *113*, 1959–1965.
(12) Park, G. S. In *Diffusion in Polymers*; Crank, J., Park, G. S., Eds.; Academic Press: London, 1968; pp 141−163.
(13) Duval, J. M.; Kemperman, A. J. B.; Folkers, B.; Mulder, M. H. V.; Desgrandchamps, G.; Smolders, C. A. *J. Appl. Polym. Sci.* **1994**, *54*, 409–418.
(14) Mahajan, R.; Koros, W. J. *Polym. Eng. Sci.* **2002**, *42*, 1420–1431.
(15) Zimmerman, C. M.; Singh, A.; Koros, W. J. *J. Membr. Sci.* **1997**, *137*, 145–154.
(16) Pomogailo, A. D. *Colloid J.* **2005**, *67*, 658–677.
(17) Ding, H.; Kumar Ram, M.; Nicolini, C. *J. Mater. Chem.* **2002**, *12*, 3585–3590.
(18) Xiong, M. N.; Zhou, S. X.; Wu, L. M.; Wang, B.; Yang, L. *Polymer* **2004**, *45*, 8127–8138.
(19) Huang, H. H.; Orler, B.; Wilkes, G. L. *Macromolecules* **1987**, *20*, 1322–1330.
(20) Khaled, S. M.; Sui, R.; Charpentier, P. A.; Rizkalla, A. S. *Langmuir* **2007**, *23*, 3988–3995.
(21) Wang, S. H.; Ahmad, Z.; Mark, J. E. *Polym. Bull.* **1993**, *31*, 323–330.
(22) Wang, S. H.; Ahmad, Z.; Mark, J. E. *Macromol. Rep.* **1994**, *A31* (Suppl. 3/4), 411–419.
(23) Wang, S. H.; Ahmad, Z.; Mark, J. E. *Chem. Mater.* **1994**, *6*, 943–946.
(24) Zheng, J. Z.; Zhou, X. P.; Xie, X. L.; Mai, Y. W. *Nanoscale* **2010**, *2*, 2269–2274.
(25) Iketani, K.; Sun, R. D.; Toki, M.; Hirota, K.; Yamaguchi, O. *J. Phys. Chem. Solids* **2003**, *64*, 507–513.
(26) Jose, N. M.; Prado, L. *Quim. Nova* **2005**, *28*, 281–288.
(27) Mammeri, F.; Le Bourhis, E.; Rozes, L.; Sanchez, C. *J. Mater. Chem.* **2005**, *15*, 3787–3811.
(28) Kierys, A.; Dziadosz, M.; Goworek, J. *J. Colloid Interface Sci.* **2010**, *349*, 361–365.
(29) Fitzgerald, J. J.; Landry, C. J. T.; Pochan, J. M. *Macromolecules* **1992**, *25*, 3715–3722.
(30) Nandi, M.; Conklin, J. A.; Salvati., L., Jr.; Sen, A. *Chem. Mater.* **1991**, *3*, 201–206.
(31) Wu, C. S. *J. Appl. Polym. Sci.* **2004**, *92*, 1749–1757.
(32) Joseph, J.; Tseng, C. Y.; Pan, C. J.; Chen, H. M.; Lin, C. W.; Pillai, K. C.; Hwang, B. J. *Polymer* **2010**, *51*, 5663–5668.
(33) Luo, M. L.; Tang, W.; Zhao, J. Q.; Pu, C. S. *J. Mater. Process. Technol.* **2006**, *172*, 431–436.
(34) Hu, Q.; Marand, E. *Polymer* **1999**, *40*, 4833–4843.
(35) Goizet, S.; Schrotter, J. C.; Smaihi, M.; Deratani, A. *New J. Chem.* **1997**, *21*, 461–468.
(36) Mazzocchetti, L.; Scandola, M.; Pollicino, A. *Polymer* **2008**, *49*, 5215–5224.
(37) Huang, Z. M.; Zhang, Y. Z.; Kotaki, M.; Ramakrishna, S. *Compos. Sci. Technol.* **2003**, *63*, 2223–2253.
(38) Li, D.; Xia, Y. N. *Adv. Mater.* **2004**, *16*, 1151–1170.
(39) Greiner, A.; Wendorff, J. H. *Angew. Chem., Int. Ed.* **2007**, *46*, 5670–5703.
(40) Pham, Q. P.; Sharma, U.; Mikos, A. G. *Tissue Eng.* **2006**, *12*, 1197–1211.
(41) Burger, C.; Hsiao, B. S.; Chu, B. *Annu. Rev. Mater. Res.* **2006**, *36*, 333–368.
(42) Barnes, C. P.; Sell, S. A.; Boland, E. D.; Simpson, D. G.; Bowlin, G. L. *Adv. Drug Delivery Rev.* **2007**, *59*, 1413–1433.
(43) Liang, D.; Hsiao, B. S.; Chu, B. *Adv. Drug Delivery Rev.* **2007**, *59*, 1392–1412.
(44) Xie, J. W.; Li, X. R.; Xia, Y. N. *Macromol. Rapid Commun.* **2008**, *29*, 1775–1792.
(45) Zukalova, M.; Prochazka, J.; Bastl, Z.; Duchoslav, J.; Rubacek, L.; Havlicek, D.; Kavan, L. *Chem. Mater.* **2010**, *22*, 4045–4055.
(46) Li, H. P.; Zhang, W.; Li, B.; Pan, W. *J. Am. Ceram. Soc.* **2010**, *93*, 2503–2506.
(47) Lee, J. A.; Krogman, K. C.; Ma, M. L.; Hill, R. M.; Hammond, P. T.; Rutledge, G. C. *Adv. Mater.* **2009**, *21*, 1252–1256.
(48) Li, D.; Xia, Y. N. *Nano Lett.* **2003**, *3*, 555–560.
(49) Lu, X. F.; Li, L. L.; Zhang, W. J.; Wang, C. *Nanotechnology* **2005**, *16*, 2233–2237.
(50) Lu, X. F.; Zhang, W. J.; Zhao, Q. D.; Wang, L. F.; Wang, C. *e-Polym.* **2006**, *033*, xxx.
(51) Wang, Y. Z.; Li, Y. X.; Yang, S. T.; Zhang, G. L.; An, D. M.; Wang, C.; Yang, Q. B.; Chen, X. S.; Jing, X. B.; Wei, Y. *Nanotechnology* **2006**, *17*, 3304–3307.
(52) Jin, W. J.; Lee, H. K.; Jeong, E. H.; Park, W. H.; Youk, J. H. *Macromol. Rapid Commun.* **2005**, *26*, 1903–1907.
(53) Ostermann, R.; Li, D.; Yin, Y. D.; McCann, J. T.; Xia, Y. N. *Nano Lett.* **2006**, *6*, 1297–1302.
(54) Hong, Y. L.; Li, D. M.; Zheng, J.; Zou, G. T. *Langmuir* **2006**, *22*, 7331–7334.
(55) Meng, X. F.; Luo, N.; Cao, S. L.; Zhang, S. M.; Yang, M. S.; Hu, X. *Mater. Lett.* **2009**, *63*, 1401–1403.
(56) Zhang, J. H.; Maurer, F. H. J.; Yang, M. S. *J. Phys. Chem. C* **2011**, *115*, 10431–10441.
(57) Zax, D. B.; Yang, D. K.; Santos, R. A.; Hegemann, H.; Giannelis, E. P.; Manias, E. *J. Chem. Phys.* **2000**, *112*, 2945–2951.
(58) Litvinov, V. M.; Spiess, H. W. *Macromol. Chem.* **1991**, *192*, 3005–3019.
(59) Kwiatkowski, J.; Whittaker, A. K. *J. Polym. Sci., Part B: Polym. Phys.* **2001**, *39*, 1678–1685.
(60) Kirst, K. U.; Kremer, F.; Litvinov, V. M. *Macromolecules* **1993**, *26*, 975–980.
(61) Anastasiadis, S. H.; Karatasos, K.; Vlachos, G.; Manias., E.; Giannelis, E. P. *Phys. Rev. Lett.* **2000**, *84*, 915–918.
(62) Krishnamoorti, R.; Vaia, R. A.; Giannelis, E. P. *Chem. Mater.* **1996**, *8*, 1728–1734.
(63) Vaia, R. A.; Sauer, B. B.; Tse, O. K.; Giannelis, E. P. *J. Polym. Sci., Part B: Polym. Phys.* **1997**, *35*, 59–67.
(64) Yim, A.; St. Pierre, L. E. *Polym. Lett.* **1969**, *7*, 237–239.
(65) Winberg, P.; Eldrup, M.; Maurer, F. H. J. *Polymer* **2004**, *45*, 8253–8264.
(66) Algers, J.; Suzuki, R.; Ohdaira, T.; Maurer, F. H. J. *Macromolecules* **2004**, *37*, 4201–4210.
(67) He, C.; Hamada, E.; Suzuki, T.; Kobayashi, H.; Kondo, K.; Shantarovich, V. P.; Ito, Y. *J. Radioanal. Nucl. Chem.* **2003**, *255*, 431–435.
(68) Algers, J.; Suzuki, R.; Ohdaira, T.; Maurer, F. H. J. *Polymer* **2004**, *45*, 4533–4539.
(69) Jean, Y. C.; Cao, H.; Dai, G. H.; Suzuki, R.; Ohdaira, T.; Kobayashi, Y.; Hirata, K. *Appl. Surf. Sci.* **1997**, *116*, 251–255.
(70) Awad, S.; Chen, H.; Chen, G.; Gu, X.; Lee, J. L.; Abdel-Hady, E. E.; Jean, Y. C. *Macromolecules* **2010**, *44*, 29–38.
(71) Jean, Y. C.; Schrader, D. M. In *Positron and Positronium Chemistry*; Schrader, D. M., Jean, Y. C., Eds.; Elsevier: Amsterdam, 1988; pp 91−117.
(72) Eldrup, M.; Lightbody, D.; Sherwood, J. N. *Chem. Phys.* **1981**, *63*, 51–58.
(73) Tao, S. J. *J. Chem. Phys.* **1972**, *56*, 5499–5510.
(74) Nakanishi, H.; Jean, Y. C. In *Positron and Positronium Chemistry*; Schrader, D. M., Jean, Y. C., Eds.; Elsevier: Amsterdam, 1988; pp 159−192.
(75) Mogensen, O. E. *J. Chem. Phys.* **1974**, *60*, 998–1004.
(76) Mogensen, O. E. *Positron Annihilation in Chemistry*; Springer-Verlag: Berlin, 1995.
(77) Wästlund, C.; Maurer, F. H. J. *Polymer* **1998**, *39*, 2897–2902.
(78) Welander, M.; Maurer, F. H. J. *J. Mater. Sci. Forum* **1992**, *105−110*, 1811–1814.
(79) Suzuki, T.; Miura, T.; Oki, Y.; Numajiri, M.; Kondo, K.; Ito, Y. *Radiat. Phys. Chem.* **1995**, *45*, 657–663.

(80) Wang, C. L.; Hirade, T.; Maurer, F. H. J.; Eldrup, M.; Pedersen, N. J. *J. Chem. Phys.* **1998**, *108*, 4654–4661.
(81) Peng, Z. L.; Olson, B. G.; McGervey, J. D.; Jamieson, A. M. *Polymer* **1999**, *40*, 3033–3040.
(82) Hirade, T.; Maurer, F. H. J.; Eldrup, M. *Radiat. Phys. Chem.* **2000**, *58*, 465–471.
(83) Ito, Y. Radiation chemistry: intraspur effects and positronium formation mechanisms. In *Positron and Positronium Chemistry*; Schrader, D. M., Jean, Y. C., Eds.; Elsevier: Amsterdam,1988; Vol. 57, pp 120−158.
(84) Kobayashi, Y.; Wang, C. L.; Hirata, K.; Zheng, W.; Zhang, C. *Phys. Rev. B: Condens. Matter Mater. Phys.* **1998**, *58*, 5384–5389.
(85) Schrader, D. M. Theoretical aspects of positronic systems. In *Positron and Positronium Chemistry*; Schrader, D. M., Jean, Y. C., Eds.; Elsevier: Amsterdam, 1988; Vol. 57, pp 27−90.
(86) Li, X. S.; Boyce, M. C. *J. Polym. Sci., Part B: Polym. Phys.* **1993**, *31*, 869–873.
(87) Dlubek, G. In *Polymer Physics: From Suspensions to Nanocomposites and Beyond*; Utracki, L. A., Jamieson, A. M., Eds.; John Wiley & Sons: New York, 2010; p 421.
(88) Schmidt, M.; Maurer, F. H. J. *Macromolecules* **2000**, *33*, 3879–3891.
(89) Schmidt, M.; Maurer, F. H. J. *Polymer* **2000**, *41*, 8419–8424.
(90) Maurer, F. H. J.; Schmidt, M. *Radiat. Phys. Chem.* **2000**, *58*, 509–512.
(91) Schmidt, M.; Maurer, F. H. J. *J. Polym. Sci., Part B: Polym. Phys.* **1998**, *36*, 1061–1080.
(92) Merkel, T. C.; Freeman, B. D.; Spontak, R. J.; He, Z.; Pinnau, I.; Meakin, P.; Hill, A. J. *Science* **2002**, *296*, 519–522.
(93) Merkel, T. C.; Freeman, B. D.; Spontak, R. J.; He, Z.; Pinnau, I.; Meakin, P.; Hill, A. J. *Chem. Mater.* **2003**, *15*, 109–123.
(94) Merkel, T. C.; He, Z. J.; Pinnau, I.; Freeman, B. D.; Meakin, P.; Hill, A. J. *Macromolecules* **2003**, *36*, 8406–8414.
(95) Merkel, T. C.; He, Z. J.; Pinnau, I.; Freeman, B. D.; Meakin, P.; Hill, A. J. *Macromolecules* **2003**, *36*, 6844–6855.
(96) Winberg, P.; DeSitter, K.; Dotremont, C.; Mullens, S.; Vankelecom, I. F. J.; Maurer, F. H. J. *Macromolecules* **2005**, *38*, 3776–3782.
(97) Anastasiadis, S. H.; Karatasos, K.; Vlachos, G.; Manias, E.; Giannelis, E. P. *Phys. Rev. Lett.* **2000**, *84*, 915–918.
(98) Giannelis, E. P. *Adv. Mater.* **1996**, *8*, 29–35.
(99) Giannelis, E. P.; Krishnamoorti, R.; Manias, E. *Adv. Polym. Sci.* **1999**, *138*, 107–47.
(100) Vaia, R. A.; Sauer, B. B.; Tse, O. K.; Giannelis, E. P. *J. Polym. Sci., Part B: Polym. Phys.* **1997**, *35*, 59–67.
(101) Lu, H. B.; Nutt, S. *Macromolecules* **2003**, *36*, 4010–4016.
(102) Hu, X. S.; Zhang, W. H.; Si, M. Y.; Gelfer, M.; Hsiao, B.; Rafailovich, M. *Macromolecules* **2003**, *36*, 823–829.
(103) Winberg, P.; Eldrup, M.; Pedersen, N. J.; van Es, M. A.; Maurer, F. H. J. *Polymer* **2005**, *46*, 8239–8249.
(104) West, D. H. D.; McBrierty, V. J.; Delaney., C. F. G. *Appl. Phys.* **1979**, *18*, 85–92.
(105) Jamieson, A. M.; Olson, B. G.; Nazarenko, S. In *Polymer Physics: From Suspensions to Nanocomposites and Beyond*; Utracki, L. A., Jamieson, A. M., Eds.; John Wiley & Sons: New York, 2010; p473.
(106) Utracki, L. A. In *Polymer Physics: From Suspensions to Nanocomposites and Beyond*; Utracki, L. A., Jamieson, A. M., Eds.; John Wiley & Sons: New York, 2010; p 553.
(107) Maurer, F. H. J.; Welander, M. *J. Adhes. Sci. Technol.* **1991**, *5*, 425–437.
(108) Hamielec, A. E.; Eldrup, M.; Mogensen, O.; Jansen, P. *J. Macromol. Sci., Rev. Macromol. Chem. Phys.* **1973**, *C9*, 305–337.
(109) Hench, L. L.; West, J. K. *Chem. Rev.* **1990**, *90*, 33–72.
(110) Wang, C. C.; Ying, J. Y. *Chem. Mater.* **1999**, *11*, 3113–3120.
(111) Fitzgerald, J. J.; Landry, C. J. T. *Macromolecules* **1992**, *25*, 3715–3722.
(112) Gillham, J. K. *Polym. Eng. Sci.* **1986**, *26*, 1429–1433.
(113) Hirata, K.; Kobayashi, Y.; Ujihira, Y. *J. Chem. Soc., Faraday Trans.* **1997**, *93*, 139–142.